Neutron Diffraction Study of the Structural and Electronic Properties of $Sr_2HoMn_2O_7$ and $Sr_2YMn_2O_7$

Peter D. Battle,* Julie E. Millburn, Matthew J. Rosseinsky,* Lauren E. Spring, and Jaap F. Vente

Inorganic Chemistry Laboratory, Oxford University, South Parks Road, Oxford, OX1 3QR, U.K.

Paolo G. Radaelli

Institut Laue-Langevin, BP 156X, 38042 Grenoble Cedex 9, France

Received June 16, 1997. Revised Manuscript Received August 26, 1997[⊗]

The crystal structures of $Sr_2HoMn_2O_7$ and $Sr_2YMn_2O_7$ have been determined at 290 and 1.7 K from neutron and X-ray powder diffraction data. Both are distorted Ruddlesden−Popper structures formed by the intergrowth of rock-salt-like layers and perovskite-like blocks of tilted MnO_6 octahedra (space group $P4_2/mnm$; for Ho at 290 K $a = 5.40388(5)$, $c = 19.9050(2)$ Å). The majority of the lanthanide cations are located in the rock-salt layers. Neither structure changes significantly on cooling to 1.7 K. There is evidence for neither charge ordering of Mn^{3+} and Mn^{4+} cations nor for long-range magnetic ordering. The magnetic susceptibility maximum observed previously is thus confirmed as signifying a transition to a spin-glass phase. The behavior of these compounds is contrasted with that of other Mn oxides which show long-range magnetic order and colossal magnetoresistance.

Introduction

Recent research into the magnetoresistance of mixed-valence manganese oxides has highlighted the extent to which the electronic properties of these compounds are controlled by their chemistry. This is readily illustrated by the significant differences between the behavior of, for example, the two perovskites $La_{0.5}Sr_{0.5}MnO_3$ and $Pr_{0.5}Sr_{0.5}MnO_3$.[1,2] A number of factors have been considered in the search for an explanation of these differences, among them cation size,[3] cation disorder,[4] and cation acidity.[5] Each of these influences the degree of orbital overlap and hence the width of the d-bands associated with the transition-metal sublattice. The ratio of lanthanide to alkaline earth controls the mean oxidation state of the Mn cations and hence the degree to which the d bands are occupied. The same factors control the behavior of the perovskite-related Ruddlesden−Popper (RP) phases (Figure 1), which have the general formula $Sr_{2-x}Ln_{1+x}Mn_2O_7$ (Ln is a lanthanide element or yttrium). However, in contrast to the situation in the 3-dimensional perovskite structure, two distinct sites are available for Ln and Sr cations in this quasi 2-dimensional crystal structure; a relatively large, 12-coordinate site (Sr/Ln1) is situated within the perovskite-like blocks, and a smaller, 9-coordinate site (Sr/Ln2) is situated on the edge of the blocks in what is often referred to as the rock-salt layer. The availability of two sites introduces an additional parameter which has an influence over the properties of these phases, namely, the degree of cation ordering on the Sr/Ln sublattice. X-ray powder diffraction has been used to monitor the variation in the degree of ordering with Ln cation[6−8] and these experiments showed that the dis-

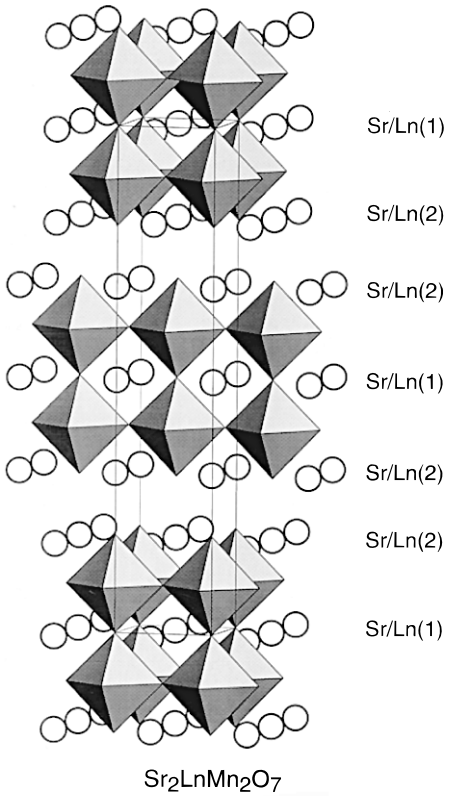

Figure 1. Crystal structure of $Sr_2LnMn_2O_7$ (space group $I4/mmm$). Octahedra represent MnO_6 groups.

[⊗] Abstract published in *Advance ACS Abstracts,* October 15, 1997.

(1) Urushibara, A.; Moritomo, Y.; Arima, T.; Asamitsu, A.; Kido, G.; Tokura, Y. *Phys. Rev. B* **1995**, *51*, 14103.
(2) Tomioka, Y.; Asamitsu, A.; Moritomo, Y.; Kuwahara, K.; Tokura, Y. *Phys. Rev. Lett.* **1995**, *74*, 5108.
(3) Mahesh, R.; Mahendiran, R.; Raychaudhuri, A. K.; Rao, C. N. R. *J. Solid State Chem.* **1995**, *120*, 204.
(4) Rodriguez-Martinez, L. M.; Attfield, J. P. *Phys. Rev. B* **1996**, *54*, R15622.
(5) Battle, P. D.; Green, M. A.; Laskey, N. S.; Kasmir, N.; Millburn, J. E.; Spring, L. E.; Sullivan, S. P.; Rosseinsky, M. J.; Vente, J. F. *J. Mater. Chem.* **1997**, *7*, 977.

S0897-4756(97)00431-6 CCC: $14.00 Published 1997 by the American Chemical Society

tribution of Sr and Ln cations over the 12- and 9-coordinate sites is essentially random when Ln = Pr or Nd but that there is, predictably, an increasing tendency for the trivalent cation to occupy the smaller, nine-coordinate sites as the cation radius of Ln^{3+} decreases. $Sr_2LaMn_2O_7$ is somewhat unusual in that the La cations preferentially occupy the 12-coordinate site; this observation implies that the size difference between Sr^{2+} and La^{3+} is sufficiently small for the distribution of cations to be determined by charge considerations. Unfortunately, the significance of the overall trend in cation ordering is rendered somewhat ambiguous by the observation[8−10] that samples containing the larger Ln cations are actually biphasic, although both of the phases present adopt the RP structure, and the differences in their structural chemistry are very subtle. However, the extent of cation ordering and the (probably related) increased stability of monophasic samples are tracked by the composition-dependent changes in electronic properties that occur in Sr_2LnMnO_7. This is illustrated by the observation of colossal magnetoresistance (CMR) at low temperatures (<126 K) in the metallic, ferromagnetic phase of a biphasic sample of bulk composition $Sr_2LaMn_2O_7$,[7,11] the observation of CMR in the absence of ferromagnetism in nonmetallic, biphasic samples having Ln = Nd,[12] and the absence of both ferromagnetism and CMR (for $0 < B/T < 14$) in nonmetallic, apparently single-phase samples containing small lanthanides.[10] To date, neutron diffraction has been used only in the characterization of Ln = La and Nd,[9,13] but magnetization measurements made for Ln = Gd, Tb, Dy, Ho, and Er show[5] evidence for neither a Néel nor a Curie point, although some hysteresis is apparent below 30 K. The susceptibility of $Sr_2YMn_2O_7$, in which the Y^{3+} cation is diamagnetic, behaves in the manner of a spin glass, implying that the Mn magnetic moments freeze at low temperatures (T_g = 17 K). We have previously[5] suggested that the Mn sublattice in the compounds Ln = Gd, Tb, Dy, Ho, and Er behaves in the same way but that the susceptibility maximum associated with the glass transition is masked by the large contribution from the Ln cations, which remain paramagnetic at temperatures down to 5 K.

To date, more attention has been paid to the RP phases containing the larger lanthanides (Ln = La, Pr, Nd), which do show CMR, than to those containing the smaller lanthanides which do not. In this paper we attempt to redress the balance somewhat by describing the results of neutron powder diffraction experiments carried out on $Sr_2LnMn_2O_7$ for Ln = Y, Ho. Our primary aim was to investigate whether charge ordering occurs between Mn^{3+} and Mn^{4+} cations in these compounds, previous experiments on perovskites[2] having established that this would be compatible with the absence of CMR. Our second objective was to establish whether or not long-range magnetic order is present at low temperatures and hence to establish whether or not these compositions are correctly described as spin glasses.

Table 1. Heating Times (h) at Various Temperatures (°C) in the Synthesis of $Sr_2LnMn_2O_7$, Ln = Ho, Y

	temp (°C)						
Ln	800	1000	1200	1250	1300	1350	1400
Ho	26	24	24	24	408	240	40
Y	32	42	120		432	240	

Experimental Section

Polycrystalline samples of $Sr_2LnMn_2O_7$ (Ln = Ho, Y) were prepared by firing the appropriate stoichiometric quantities of dried Ln_2O_3, $SrCO_3$, and MnO_2 in air under the conditions specified in Table 1. The reactants were ground and repelletized at regular intervals during the firing cycle, and the progress of the reactions was monitored by X-ray powder diffraction. In view of the known propensity[8] of these materials to form mixtures containing two essentially isostructural phases, considerable care was taken to ensure that these relatively large samples (~10 g each) were homogeneous and highly crystalline. This was done by monitoring both the shape and width of the {0 0 10} Bragg peak, which does not split even if the symmetry falls below that expected (tetragonal). The syntheses were deemed to be complete when the diffraction patterns collected on a Siemens D5000 diffractometer, operating in Bragg−Brentano geometry with Cu $K\alpha_1$ radiation, satisfied two criteria: first that they contained a symmetrical {0 0 10} reflection having a fwhm < 0.1° (2θ), and second that the complete pattern ($10 < 2\theta/° < 100$) could be fitted in a Rietveld analysis[14] with only one RP phase in the structural model. The detector was moved with a step size $\Delta 2\theta = 0.01°$ when analyzing the width of {0 0 10}, and $\Delta 2\theta = 0.02°$ when collecting a full diffraction pattern for profile analysis. To avoid the pitfalls encountered in our study of $Sr_2LaMn_2O_7$,[13,15] we carried out further analysis of the {0 0 10} peak shape on the high-resolution powder diffractometer 2.3 at SRS, Daresbury Laboratory. The fwhm determined on this instrument by fitting to a single pseudo-Voigt function were 0.077(1)° (Ho) and 0.086(1)° (Y), values that were low enough to convince us that only one RP phase is present in these samples. SQUID magnetometry was used to confirm that they have the same magnetic properties as the smaller batches that were used in previous characterizations.[5] Iodometric titrations resulted in a value of 3.51(1) for the mean oxidation state of Mn in both $Sr_2HoMn_2O_7$ and $Sr_2YMn_2O_7$. Neutron powder diffraction data were collected in the temperature range $1.5 \leq T/K \leq 293$ using the powder diffractometers D1b (λ = 2.520 Å, $5 \leq 2\theta/° \leq 85$, $\Delta 2\theta = 0.2°$) and D2b (λ = 1.59412 Å, $5 \leq 2\theta/° \leq 150$, $\Delta 2\theta = 0.05°$) at ILL, Grenoble. Samples were contained in cylindrical vanadium cans. All neutron diffraction patterns were analysed with the program package GSAS,[16] using the following scattering lengths: $b_{Sr} = 0.702$, $b_{Ho} = 0.808$, $b_Y = 0.775$, $b_{Mn} = -0.373$, and $b_O = 0.5805 \times 10^{-14}$ m. The background was fitted with a first-order Chebychev polyno-

(6) Seshadri, R.; Martin, C.; Hervieu, M.; Raveau, B.; Rao, C. N. R. *Chem. Mater.* **1997**, *9*, 270.
(7) Seshadri, R.; Martin, C.; Maignan, A.; Hervieu, M.; Raveau, B.; Rao, C. N. R. *J. Mater. Chem.* **1996**, *6*, 1585.
(8) Battle, P. D.; Green, M. A.; Laskey, N. S.; Millburn, J. E.; Murphy, L.; Rosseinsky, M. J.; Sullivan, S. P.; Vente, J. F. *Chem. Mater.* **1997**, *9*, 552.
(9) Battle, P. D.; Green, M. A.; Laskey, N. S.; Millburn, J. E.; Radaelli, P. G.; Rosseinsky, M. J.; Sullivan, S. P.; Vente, J. F. *Phys. Rev. B* **1996**, *54*, 15967.
(10) Battle, P. D.; Blundell, S. J.; Cox, D. E.; Green, M. A.; Millburn, J. E.; Radaelli, P. G.; Rosseinsky, M. J.; Singleton, J.; Spring, L. E.; Vente, J. F. *MRS Symp. Proc.* **1997**, *453*, 331.
(11) Moritomo, Y.; Asamitsu, A.; Kuwahara, H.; Tokura, Y. *Nature* **1996**, *380*, 141.
(12) Battle, P. D.; Blundell, S. J.; Green, M. A.; Hayes, W.; Honold, M.; Klehe, A. K.; Laskey, N. S.; Millburn, J. E.; Murphy, L.; Rosseinsky, M. J.; Samarin, N. A.; Singleton, J.; Sluchanko, N. A.; Sullivan, S. P.; Vente, J. F. *J. Phys.: Condensed Matter* **1996**, *8*, L427.
(13) Battle, P. D.; Cox, D. E.; Green, M. A.; Millburn, J. E.; Spring, L. E.; Radaelli, P. G.; Rosseinsky, M. J.; Vente, J. F. *Chem. Mater.* **1997**, *9*, 1042.
(14) Rietveld, H. M. *J. Appl. Crystallogr.* **1969**, *2*, 65.
(15) Battle, P. D.; Green, M. A.; Laskey, N. S.; Millburn, J. E.; Rosseinsky, M. J.; Sullivan, S. P.; Vente, J. F. *Chem. Commun.* **1996**, 767.
(16) Larson, A. C.; von Dreele, R. B. General Structure Analysis System (GSAS), Los Alamos National Laboratories, Report LAUR 86-748, 1990.

Table 2. Generalized Crystallography for the Ruddelsden−Popper Structure in Space Group $P4_2/mnm$, No. 136, $Z = 4$

atom	site	coordinates	
Sr/Ln1	4f	$x\ x\ 0$	$x \sim 1/4$
Sr/Ln2	8j	$x\ x\ z$	$x \sim 1/4$, $z \sim 0.2$
Mn	8j	$x\ x\ z$	$x \sim 1/4$, $z \sim 0.4$
O1	4g	$x\ -x\ 0$	$x \sim 1/4$
O2	8j	$x\ x\ z$	$x \sim 1/4$, $z \sim 0.3$
O3	8h	$0\ 1/2\ z$	$z \sim 0.1$
O4	4e	$0\ 0\ z$	$z \sim 0.1$
O5	4e	$0\ 0\ z$	$z \sim 0.4$

mial, and the shape of the Bragg peaks was described by a five-term pseudo-Voigt function. In view of the results of the chemical analysis, the anion sublattice was constrained to be fully occupied. A full X-ray powder diffraction pattern of $Sr_2HoMn_2O_7$ was collected at room temperature on Station 2.3 at SRS, Daresbury Laboratory. A wavelength $\lambda = 1.40096(2)$ Å was used to collect data over the angular range $15 \leq 2\theta/° \leq 100$ with a stepsize $\Delta 2\theta = 0.01°$. In the analysis of these data, a four-term pseudo-Voigt was used to describe the peak shape, and a first-order Chebyshev polynomial to describe the background level. In addition, slow scans were carried out over angular regions where additional peaks might be expected if the symmetry of the structure had previously been over estimated. No such peaks, which could be caused by charge ordering, were seen.

Results

Although the X-ray characterization described above indicated that our samples of $Sr_2HoMn_2O_7$ and $Sr_2YMn_2O_7$ were monophasic, inspection of neutron diffraction data collected at room temperature on D2b showed that this conclusion was incorrect. A number of weak, unexpected Bragg peaks were observed, some of which could be indexed in a primitive tetragonal unit cell with $a \sim \sqrt{2}a_x$, $c \sim c_x$ where a_x and c_x are the unit cell parameters of the ideal, body-centered RP unit cell (Figure 1) identified in the X-ray experiments and observed previously in the case of, for example, $Sr_2NdMn_2O_7$. However, some of the relatively weak Bragg peaks could not be accounted for in this enlarged unit cell, although they could be accounted for by an orthorhombic unit cell of size ~5.4 × 7.8 × 5.4 Å, indicating the presence of a small amount of perovskite. We therefore analyzed our data using a model that was based on a distorted RP phase with a tetragonal unit cell of size ~5.4 × 19.9 Å in space group $P4_2/mnm$ but that included a minority perovskite phase (~3 wt %). We attempted to refine the structure of the RP phase in orthorhombic and monoclinic space groups which would be consistent with charge-ordering of the Mn^{3+} and Mn^{4+} cations and tilting of the MnO_6 octahedra, but it became clear that this approach was inconsistent with the data. There was no evidence of a further symmetry reduction below the tetragonal space group $P4_2/mnm$, and our final refinements were carried out using this space group, which allows only one Mn site (Table 2) and thus disallows charge ordering. However, compared to the space group ($I4/mmm$) of the ideal structure, $P4_2/mnm$ does give some additional freedom to the MnO_6 octahedra, in terms of both orientation and the number of independent Mn−O bond lengths. The latter is increased from three to five as the point symmetry at the Mn site is reduced from $4mm$ to m. This reduction, together with the increase in the numbers of degrees of freedom on the oxide sublattice, leads to considerable nonlinearity in Mn−O−Mn bond angles. These strongly influence the strength of the superexchange interaction, and hence the magnetic properties of the compound. There is also a significant increase in the number of independent bond lengths around the Sr/Ln1 and Sr/Ln2 sites. A similar distortion has been seen previously in $Sr_2TbFe_2O_7$.[17] In the case of $Sr_2HoMn_2O_7$, we performed a structure refinement making simultaneous use of X-ray (2.3, SRS) and neutron (D2b) data in order to improve the precision of the cation distribution on sites Sr/Ho1 and Sr/Ho2; the isoelectronic nature of Sr^{2+} and Y^{3+} rendered this approach pointless in the case of $Sr_2YMn_2O_7$ and, because their neutron scattering lengths are also very similar, we simply assumed that the Y^{3+} cations occupy 50% of the Sr/Y2 sites within the rock-salt layers of the RP structure. We believe this to be a reasonable assumption in view of the refined Sr/Ho distribution and the similar ionic radii of Y^{3+} and Ho^{3+}. In each case the perovskite phase (~3 wt %) was modeled in space group $Pnma$; we do not attach any significance to the refined structural parameters of this phase, although its inclusion in the model facilitated the structural refinement of the majority phase. Isotropic temperature factors were adequate to describe the thermal motion of the cations in the majority phase, but there was evidence of anisotropy on the anion sublattice. Most notably, the oxide ions O3, O4, and O5 show enhanced motion parallel to z, that is perpendicular to the equatorial plane around Mn which they define. The refined structural parameters and the agreement indices are listed in Table 3 (Ho) and Table 4 (Y), with the most significant bond lengths and bond angles in Tables 5 and 6, respectively. The observed and calculated neutron diffraction profiles are shown in Figures 2 and 3. Data collected at 1.7 K showed very few differences from those collected at room temperature, with no indication of magnetic Bragg scattering at low temperature. They were analyzed in a manner similar to that described above, although no X-ray data were used in the analysis of the Ho-containing structure, the cation distribution being held fixed in the high-temperature configuration. The results of these refinements are presented in Tables 7−10. Figure 4 shows the low-angle diffraction data collected on D1b at 2 K and also the difference between these data and those collected at 250 K. Although the absence of magnetic Bragg peaks rules out the possibility of long-range magnetic order, the low-temperature enhancement of the diffuse scattering in the region $15 < 2\theta/° < 30$ suggests that short-range spin ordering does occur; this effect was apparent in data collected on $Sr_2YMn_2O_7$ at temperatures below 110 K. The diffuse maximum is centered at a 2θ value close to that where the {003} reflection would occur. This is one of the strongest magnetic Bragg peaks in both $Sr_{2.04}La_{0.96}Mn_2O_7$ and $Sr_2NdMn_2O_7$, and the data thus suggest that the short-range magnetic order in $Sr_2HoMn_2O_7$ and $Sr_2YMn_2O_7$ is similar to the antiferromagnetic long-range order seen in the La and Nd compounds. There is a marked difference between the data collected on the Ho and Y compounds in that the difference curve for the former goes to zero for $2\theta < 15°$, whereas that for the latter becomes negative. This can be taken as further evidence that the Ho cations in $Sr_2HoMn_2O_7$ remain

(17) Samaras, D.; Collomb, A.; Joubert, J. C. *J. Solid State Chem.* **1973**, *7*, 337.

Table 3. Crystallographic Data for $Sr_2HoMn_2O_7$ at 290 K

	x	*z*	U_{iso} (Å^2)	U_{11}[a] (Å^2)	U_{33} (Å^2)	U_{12}[b] (Å^2)
Sr/Ho1[c]	0.2520(4)	0	0.0075(3)			
Sr/Ho2[d]	0.2560(3)	0.18358(4)	0.0084(2)			
Mn	0.2513(8)	0.40171(9)	0.0010(2)			
O1	0.2339(9)	0		0.016(1)	0.010(1)	−0.002(4)
O2	0.2303(7)	0.2999(1)		0.030(1)	0.031(1)	0.006(3)
O3	0	0.1002(3)		0.004(2)	0.024(2)	−0.007(2)
O4	0	0.1086(4)		0.015(2)	0.045(4)	0.006(3)
O5	0	0.4036(3)		0.006(1)	0.015(2)	0.006(3)

$a = 5.40388(5)$ Å, $c = 19.9050(2)$ Å, $V = 581.26(2)$ Å^3
neutrons: $R_{wp} = 3.97\%$ $R_p = 2.95\%$ DWd = 0.61
X-rays $R_{wp} = 6.24\%$ $R_p = 4.32\%$ DWd = 1.17
totals $R_{wp} = 5.14\%$ $R_p = 4.14\%$ DWd = 0.99 $\chi_{red}^2 = 3.84$ for 84 variables

Perovskite Phase
$Sr_{0.5}Ho_{0.5}MnO_3$ 3.0(2)% by weight
space group *Pnma*, $a = 5.3770(5)$ Å, $b = 7.6668(9)$ Å, $c = 5.4101(5)$ Å

[a] $U_{11} = U_{22}$, except O3: $U_{22} = 0.010(2)$ Å^2. [b] $U_{13} = U_{23} = 0$, except O2: $U_{13} = U_{23} = 0.006(2)$ Å^2. [c] Ho content 12.2(5)%. [d] Ho content 43.9(3)%.

Table 4. Crystallographic Data for $Sr_2YMn_2O_7$ at 290 K

	x	*z*	U_{iso} (Å^2)	U_{11}[a] (Å^2)	U_{33} (Å^2)	U_{12}[b] (Å^2)
Sr1	0.2522(8)	0	0.0064(4)			
Sr/Y2[c]	0.2554(3)	0.18377(7)	0.0088(2)			
Mn	0.251(1)	0.4016(1)	0.0022(3)			
O1	0.2359(9)	0		0.018(1)	0.011(1)	0.005(6)
O2	0.2304(8)	0.2998(1)		0.033(1)	0.032(1)	0.004(5)
O3	0	0.1001(4)		0.010(2)	0.026(3)	−0.006(2)
O4	0	0.1074(5)		0.010(2)	0.049(5)	−0.001(3)
O5	0	0.4039(4)		0.010(2)	0.012(2)	0.002(2)

$a = 5.40456(6)$ Å, $c = 19.9054(2)$ Å, $V = 581.42(2)$ Å^3
$R_{wp} = 5.42\%$ $R_p = 4.05\%$ DWd = 0.52 $\chi_{red}^2 = 6.95$ for 65 variables

Perovskite Phase
$Sr_{0.5}Y_{0.5}MnO_3$ 2.2(1)% by weight
space group *Pnma*, $a = 5.3776(8)$ Å, $b = 7.635(2)$ Å, $c = 5.4179(8)$ Å

[a] $U_{11} = U_{22}$, except O3: $U_{22} = 0.007(2)$ Å^2. [b] $U_{13} = U_{23} = 0$, except O2: $U_{13} = U_{23} = 0.006(1)$ Å^2. [c] Y content fixed at 50%.

Table 5. Bond Lengths (Å) and Bond Angles (deg) in $Sr_2HoMn_2O_7$ at Room Temperature

Sr/Ho1−O1	2×	2.628(5)	Sr/Ho2−O2	1×	2.325(2)	Mn−O1	1×	1.959(2)
Sr/Ho1−O1	2×	2.779(5)	Sr/Ho2−O2	2×	2.861(4)	Mn−O2	1×	2.032(3)
Sr/Ho1−O3	4×	2.762(5)	Sr/Ho2−O2	2×	2.584(4)	Mn−O3	2×	1.9109(1)
Sr/Ho1−O4	2×	2.896(6)	Sr/Ho2−O3	2×	2.531(4)	Mn−O4	1×	1.912(6)
Sr/Ho1−O5	2×	2.696(6)	Sr/Ho2−O4	1×	2.460(5)	Mn−O5	1×	1.921(6)
			Sr/Ho2−O5	1×	2.547(5)			
O1−Mn−O2		178.7(6)	O2−Mn−O4		88.3(4)	O4−Mn−O5		174.9(4)
O1−Mn−O3		91.2(2)	O2−Mn−O5		86.6(4)	Mn−O1−Mn		173.4(6)
O1−Mn−O4		92.9(4)	O3−Mn−O3		177.6(4)	Mn−O3−Mn		177.7(4)
O1−Mn−O5		92.2(4)	O3−Mn−O4		90.2(2)	Mn−O4−Mn		167.6(5)
O2−Mn−O3		88.8(2)	O3−Mn−O5		89.7(2)	Mn−O5−Mn		177.7(4)

Table 6. Bond Lengths (Å) and Bond Angles (deg) in $Sr_2YMn_2O_7$ at Room Temperature

Sr1−O1	2×	2.639(6)	Sr/Y2−O2	1×	2.319(3)	Mn−O1	1×	1.962(2)
Sr1−O1	2×	2.768(6)	Sr/Y2−O2	2×	2.857(4)	Mn−O2	1×	2.030(4)
Sr1−O3	4×	2.762(6)	Sr/Y2−O2	2×	2.589(4)	Mn−O3	2×	1.9111(2)
Sr1−O4	2×	2.879(8)	Sr/Y2−O3	2×	2.534(6)	Mn−O4	1×	1.910(8)
Sr1−O5	2×	2.691(7)	Sr/Y2−O4	1×	2.474(7)	Mn−O5	1×	1.920(8)
			Sr/Y2−O5	1×	2.558(6)			
O1−Mn−O2		178.4(7)	O2−Mn−O4		90.2(2)	O4−Mn−O5		176.1(5)
O1−Mn−O3		91.0(3)	O2−Mn−O5		89.8(2)	Mn−O1−Mn		174.2(8)
O1−Mn−O4		92.5(5)	O3−Mn−O3		177.8(5)	Mn−O3−Mn		177.9(6)
O1−Mn−O5		91.5(4)	O3−Mn−O4		90.2(2)	Mn−O4−Mn		169.3(6)
O2−Mn−O3		88.9(3)	O3−Mn−O5		89.8(2)	Mn−O5−Mn		177.1(5)

paramagnetic down to 2 K. In the presence of diamagnetic Y^{3+}, short-range ordering on the Mn sublattice transfers paramagnetic scattering from the low-angle background into the broad maximum and leaves no free paramagnetic ions to contribute to the low-angle background. However, in the Ho compound, the Ho sublattice remains paramagnetic and continues to dominate the low-angle scattering at temperatures down to 2 K.

Discussion

The crystal structures described above are different from those deduced previously in X-ray studies of $Sr_2HoMn_2O_7$ and $Sr_2YMn_2O_7$.[8] This is because the deviations from the ideal body-centered RP structure are brought about principally by small displacements of the oxide ions, and neutron diffraction is more sensitive to the positions of these light atoms. The magnitude of

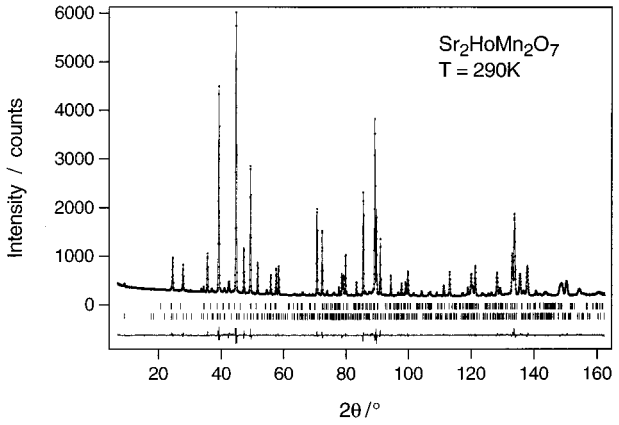

Figure 2. Observed (dots) and calculated (line) neutron powder diffraction profiles of $Sr_2HoMn_2O_7$ at 290 K. A difference curve is drawn. The upper and lower vertical lines mark reflection positions for the perovskite minority phase and $Sr_2HoMn_2O_7$ respectively.

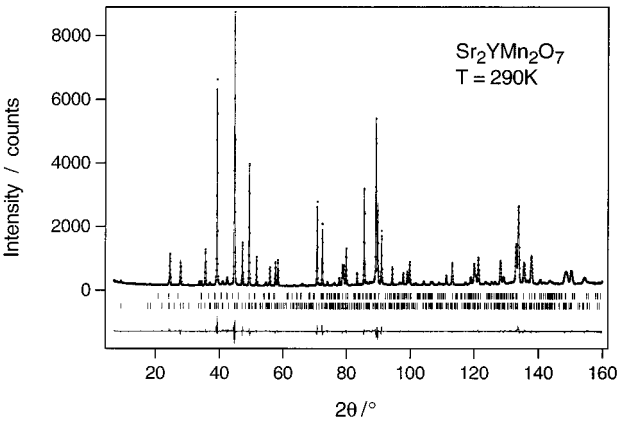

Figure 3. Observed (dots) and calculated (line) neutron powder diffraction profiles of $Sr_2YMn_2O_7$ at 290 K. A difference curve is drawn. The upper and lower vertical lines mark reflection positions for the perovskite minority phase and $Sr_2YMn_2O_7$, respectively.

the distortion can be gauged from Figure 5, which shows the atomic arrangement in a perovskite block of $Sr_2HoMn_2O_7$ viewed along two perpendicular directions; the atomic displacements are apparent only in the view, shown in Figure 5a, along a line almost parallel to O3−Mn−O3. The distortion in $Sr_2YMn_2O_7$ is of a very similar nature, and both can be likened to the tilting of BO_6 octahedra that occurs in ABO_3 perovskites when the ionic radii r_A, r_B, and r_O give rise to a tolerance factor $(r_A + r_O)/\sqrt{2}(r_B + r_O) \leqslant 1$. In the present case, where the tilt is necessary in order to satisfy the coordination requirements of the smaller Sr/Ln site, the critical ratio is $(r_{Sr/Ln2} + r_O)/\sqrt{2}(r_B + r_O)$. The orientation of the sole tilt axis (O3−Mn−O3) rotates by 90° in the *xy* plane on passing from one perovskite block to the next, and the distortion of this RP structure is therefore analogous to that seen in the low-temperature tetragonal (LTT) phase of $La_{1.875}Ba_{0.125}CuO_4$,[18] a K_2NiF_4-like structure in which the perovskite blocks are only one layer in thickness. The *R* factors in Tables 3, 4, 7, and 8 suggest that these are high-quality refinements and that the resulting parameters merit careful consideration. A comparison of the unit-cell parameters and bond lengths in the two compounds, at both 290 and 1.7 K, shows that the Ho and Y congeners are structurally very similar and that neither compound shows any significant structural change on cooling. These observations support the idea that any difference in their magnetic properties is likely to be due to the presence of unpaired electrons in the 4f shell of Ho, rather than to structural differences. Neither do the temperature factors change significantly on cooling, thus indicating that the large, albeit approximately isotropic, value refined for O2 (Figure 6) is due to static displacements rather than to thermal motion. The displacements are due to the presence of both Mn^{3+} and Mn^{4+} on the octahedral sites and to the disordered cation arrangement on the Sr/Ln2 site. It is interesting to note that the oxide ion in the rock-salt layer of the LTT form of $La_{1.875}Ba_{0.125}CuO_4$ also has a high temperature factor.[18] The remaining oxide ions in $Sr_2HoMn_2O_7$ and $Sr_2YMn_2O_7$ require more anisotropic displacements in order to accommodate the disorder, and it seems likely that the deviation from 180° of the individual Mn−O−Mn bond angles is greater than is suggested by the mean values presented in Tables 5, 6, 9, and 10. This would be expected to reduce the width of the Mn 3d bands and thus favor electron localization. In view of the differences in their physical properties, it is interesting to compare the structures of $Sr_2HoMn_2O_7$ and $Sr_2YMn_2O_7$ with that of $Sr_2NdMn_2O_7$, although it must be remembered that two RP phases were present in the best-characterized sample of the latter composition. Predictably, the introduction of the smaller lanthanide cations, Ho and Y, causes a reduction in the unit-cell volume per formula unit. However, this decrease is not isotropic, largely due to the marked increase in cation ordering over the two Sr/Ln sites. The nonrandom distribution is revealed by the increase in the mean bond length Sr/Ln1−O (the perovskite block site) which occurs on moving from $Sr_2NdMn_2O_7$ (2.712 and 2.727 Å in the majority and minority phases, respectively[9]) to $Sr_2HoMn_2O_7$ (2.754 Å), despite the decrease in the ionic radius of Ln^{3+}. The increase can be attributed to the enhanced concentration of the relatively large Sr^{2+} cations on the 12-coordinate site. The anisotropy of the concomitant distortion can be seen by considering the parallelepipeds formed by eight neighboring Mn cations in the perovskite blocks; each of these contains a Sr/Ln1 cation (Figures 1 and 5). At room temperature, this volume is essentially cubic in both phases present in $Sr_2NdMn_2O_7$, with the Mn−Mn distance being ∼3.85 Å.[9] In the case of $Sr_2HoMn_2O_7$ the volume is orthorhombic, ∼3.80 × 3.82 × 3.91 Å. The marked elongation parallel to *z*, which results in Mn−O1 bond lengths ∼0.03 Å longer than those in the Nd compound, in combination with the observed displacements of the oxide ions, allows the structure to accommodate the larger, Sr-rich Sr/Ln1 site despite the reduced volume of the parallelepiped. One obvious consequence of these changes is that the interatomic electron−electron interactions within the *xy* plane will be enhanced compared to those along the *z* axis. Furthermore, whereas exchangestriction is able to decrease the Mn−Mn distance parallel to *z* in phase 1 of $Sr_2NdMn_2O_7$, the increased size of the Sr/Ln1 site prevents such an effect occurring at low temperatures in $Sr_2HoMn_2O_7$ and $Sr_2YMn_2O_7$, and a distortion that would stabilize an antiferromagnetic ground state is therefore lost; a similar argument was

(18) Katano, S.; Fernandez-Baca, J. A.; Funahashi, S.; Môri, N.; Ueda, Y.; Koga, K. *Physica C* **1993**, *214*, 64.

Table 7. Crystallographic Data for $Sr_2HoMn_2O_7$ at 1.7 K

	x	*z*	U_{iso} (Å^2)	U_{11}[a] (Å^2)	U_{33} (Å^2)	U_{12}[b] (Å^2)
Sr/Ho1[c]	0.2537(4)	0	0.0045(4)			
Sr/Ho2[d]	0.2583(3)	0.18340(8)	0.0052(2)			
Mn	0.2512(9)	0.4014(1)	0.0015(4)			
O1	0.2336(9)	0		0.016(1)	0.012(1)	0.000(5)
O2	0.2264(8)	0.2998(1)		0.032(1)	0.029(1)	0.005(4)
O3	0	0.1004(4)		0.006(2)	0.021(2)	−0.007(2)
O4	0	0.1094(4)		0.009(2)	0.027(3)	−0.008(3)
O5	0	0.4053(4)		0.011(2)	0.006(2)	0.004(2)

$a = 5.39808(7)$ Å, $c = 19.8525(3)$ Å, $V = 578.49(2)$ Å^3
$R_{wp} = 4.53\%$, $R_p = 3.59\%$, DWd $= 0.320$ $\chi_{red}^2 = 10.5$ for 65 variables

Perovskite Phase
$Sr_{0.5}Ho_{0.5}MnO_3$ 2.8(3)% by weight
space group *Pnma*, $a = 5.3652(9)$ Å, $b = 7.622(2)$ Å, $c = 5.409(1)$ Å

[a] $U_{11} = U_{22}$, except O3: $U_{22} = 0.007(2)$ Å^2. [b] $U_{13} = U_{23} = 0$, except O2: $U_{13} = U_{23} = 0.007(1)$ Å^2. [c] Ho content fixed at 12.2%. [d] Ho content fixed at 43.9%.

Table 8. Crystallographic Data for $Sr_2YMn_2O_7$ at 1.7 K

	x	*z*	U_{iso} (Å^2)	U_{11}[a] (Å^2)	U_{33} (Å^2)	U_{12}[b] (Å^2)
Sr1	0.2530(5)	0	0.0041(4)			
Sr/Y2[c]	0.2576(3)	0.18355(9)	0.0075(3)			
Mn	0.250(1)	0.4014(1)	0.0019(4)			
O1	0.2338(9)	0		0.017(1)	0.014(1)	−0.002(5)
O2	0.2266(8)	0.3000(1)		0.031(1)	0.029(1)	0.007(4)
O3	0	0.1000(5)		0.007(2)	0.025(3)	−0.006(2)
O4	0	0.1082(5)		0.007(2)	0.029(4)	−0.006(3)
O5	0	0.4054(4)		0.013(3)	0.009(3)	0.004(3)

$a = 5.40009(8)$ Å, $c = 19.8488(3)$ Å, $V = 578.81(2)$ Å^3
$R_{wp} = 5.69\%$, $R_p = 4.43\%$, DWd $= 0.42$ $\chi_{red}^2 = 4.68$ for 65 variables

Perovskite Phase
$Sr_{0.5}Yo_{0.5}MnO_3$ 2.0(1)% by weight
space group *Pnma*, $a = 5.366(9)$ Å, $b = 7.626(2)$ Å, $c = 5.414(1)$ Å

[a] $U_{11} = U_{22}$, except O3: $U_{22} = 0.008(3)$ Å^2. [b] $U_{13} = U_{23} = 0$, except O2: $U_{13} = U_{23} = 0.006(1)$ Å^2. [c] Y content fixed at 50%.

Table 9. Bond Lengths (Å) and Bond Angles (deg) in $Sr_2HoMn_2O_7$ at 1.7 K

Sr/Ho1−O1	2×	2.632(5)	Sr/Ho2−O2	1×	2.325(3)	Mn−O1	1×	1.961(3)
Sr/Ho1−O1	2×	2.770(6)	Sr/Ho2−O2	2×	2.891(4)	Mn−O2	1×	2.024(4)
Sr/Ho1−O3	4×	2.760(6)	Sr/Ho2−O2	2×	2.550(4)	Mn−O3	2×	1.9088(2)
Sr/Ho1−O4	2×	2.909(7)	Sr/Ho2−O3	2×	2.522(5)	Mn−O4	1×	1.911(8)
Sr/Ho1−O5	2×	2.658(6)	Sr/Ho2−O4	1×	2.460(5)	Mn−O5	1×	1.920(8)
			Sr/Ho2−O5	1×	2.551(6)			
O1−Mn−O2		178.0(7)	O2−Mn−O4		88.9(4)	O4−Mn−O5		177.7(5)
O1−Mn−O3		91.1(3)	O2−Mn−O5		87.0(4)	Mn−O1−Mn		173.2(7)
O1−Mn−O4		93.0(4)	O3−Mn−O3		177.7(4)	Mn−O3−Mn		177.8(5)
O1−Mn−O5		91.1(4)	O3−Mn−O4		90.1(2)	Mn−O4−Mn		167.2(5)
O2−Mn−O3		88.9(3)	O3−Mn−O5		89.8(2)	Mn−O5−Mn		175.3(5)

Table 10. Bond Lengths (Å) and Bond Angles (deg) in $Sr_2YMn_2O_7$ at 1.7 K

Sr1−O1	2×	2.631(6)	Sr/Y2−O2	1×	2.324(3)	Mn−O1	1×	1.959(3)
Sr1−O1	2×	2.773(6)	Sr/Y2−O2	2×	2.888(4)	Mn−O2	1×	2.021(4)
Sr1−O3	4×	2.754(6)	Sr/Y2−O2	2×	2.554(4)	Mn−O3	2×	1.9095(2)
Sr1−O4	2×	2.890(8)	Sr/Y2−O3	2×	2.529(6)	Mn−O4	1×	1.917(9)
Sr1−O5	2×	2.661(7)	Sr/Y2−O4	1×	2.471(6)	Mn−O5	1×	1.913(9)
			Sr/Y2−O5	1×	2.558(7)			
O1−Mn−O2		178.4(7)	O2−Mn−O4		89.4(5)	O4−Mn−O5		176.6(5)
O1−Mn−O3		90.8(3)	O2−Mn−O5		87.2(5)	Mn−O1−Mn		172.9(8)
O1−Mn−O4		92.2(5)	O3−Mn−O3		178.2(6)	Mn−O3−Mn		178.2(6)
O1−Mn−O5		91.2(5)	O3−Mn−O4		90.0(3)	Mn−O4−Mn		168.5(6)
O2−Mn−O3		89.1(3)	O3−Mn−O5		90.0(3)	Mn−O5−Mn		175.3(5)

used to explain the absence of long-range magnetic order in phase 2 of $Sr_2NdMn_2O_7$, which has an enhanced Sr^{2+} concentration on the Sr/Ln1 site.

The absence of magnetic Bragg peaks in the diffraction patterns collected on $Sr_2HoMn_2O_7$ and $Sr_2YMn_2O_7$ at 1.7 K confirms the absence of long-range magnetic order in these materials and supports our previous description[5] of them as spin glasses. However, the angular position and temperature dependence of the maximum in the diffuse scattering suggest that some features of the magnetic structures of the La and Nd analogues may be preserved, over short distances, to temperatures well above the susceptibility maximum previously identified as the glass transition temperature. With this proviso, the results described above, taken in conjunction with those from previous work,[5,8,10] suggest that these two compounds are paramagnetic insulators at room temperature, and that the only magnetic phase transition detected in the temperature range $5 \leqslant T/K \leqslant 300$ involves the freezing of the magnetic moments on the Mn sublattice to form a spin glass phase at 15 K (Ho) or 17 K (Y). These properties

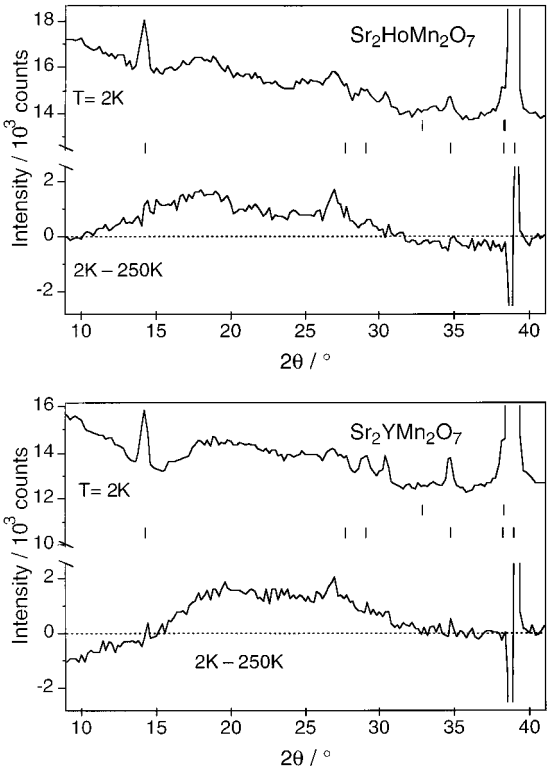

Figure 4. Low-angle diffraction data at 2 K for $Sr_2HoMn_2O_7$ (top) and $Sr_2YMn_2O_7$ (bottom). The difference between data collected at 2 and 250 K is also shown.

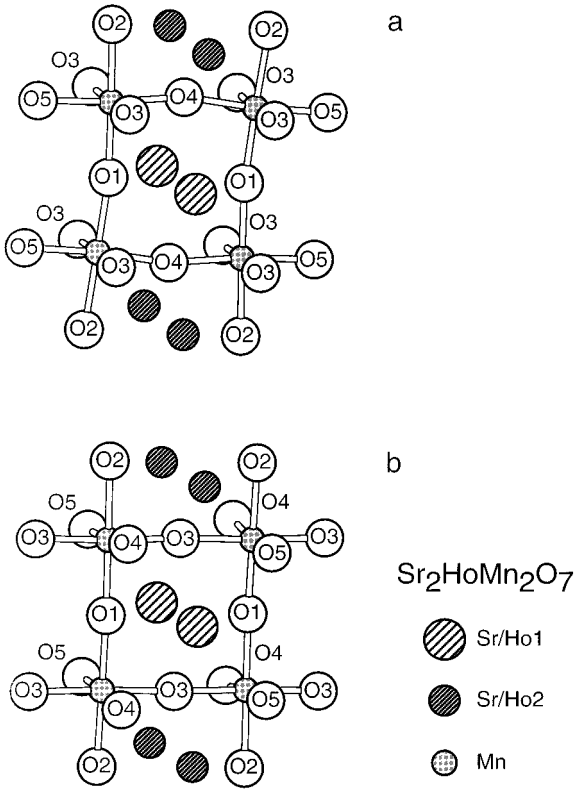

Figure 5. Atomic arrangement in $Sr_2HoMn_2O_7$ viewed along a line almost (a) parallel to O3−Mn−O3 and (b) perpendicular to O3−Mn−O3. The tilt within the bilayer is similar to that in the monolayer of LTT $La_{2-x}Ba_xCuO_4$.

apparently derive from a 1:1 assembly of Mn^{3+} and Mn^{4+} cations which are distributed in a random manner over the octahedral sites of a slightly distorted RP structure. The observation of insulating behavior in these compounds, which have a nonintegral (3.5) number of d electrons per Mn cation, implies that the 3d band is relatively narrow. The bandwidth will be determined by a number of factors, but it is likely that the increase in the nonlinearity of the Mn−O−Mn pathways, brought about by the structural distortion, will reduce orbital overlap and hence favor electron localization. In all $Sr_2LnMn_2O_7$ compounds the relatively acidic trivalent cations will compete with the Mn cations for the electron density on the anions, and this competition will limit the width of the d bands. The ordering of the trivalent cations onto the Sr/Ln2 sites ensures that they compete more effectively in $Sr_2HoMn_2O_7$ and $Sr_2YMn_2O_7$ than they do in $Sr_2NdMn_2O_7$, where more of them occupy the Sr/Ln1 site which lies further from the anions. These localizing effects appear to outweigh the delocalizing effect of the increased orbital overlap that must be brought about by the relatively short Mn−Mn distances observed in the *xy* plane. Irrespective of the cation oxidation states, the magnetic (π) interactions between the t_{2g} electrons of the Mn cations in these compounds are expected to be antiferromagnetic, as are the σ interactions between pairs of Mn^{3+} cations in this case. The observation of spin glass behavior, rather than long-range magnetic order, on this sublattice implies that frustration is introduced by the additional presence of ferromagnetic interactions. The ferromagnetic double exchange interaction will be weak because of the reduced bandwidth, and the interaction responsible for the frustration is likely to be the σ superexchange between neighboring Mn^{3+} (e_g^1) and Mn^{4+} (e_g^0) cations, although the observation of spin-glass behavior in compounds in which there is no frustration among nearest-neighbor cations, for example, Sr_2FeTaO_6, suggests that the next-nearest-neighbor interactions should not be ignored,[19] particularly in view of the short intercation distance in the *xy* plane of the Ho and Y compounds. There is a clear difference between the spin glass phase of $Sr_2HoMn_2O_7$ and that (phase 2) of $Sr_2NdMn_2O_7$ in that the Nd spins

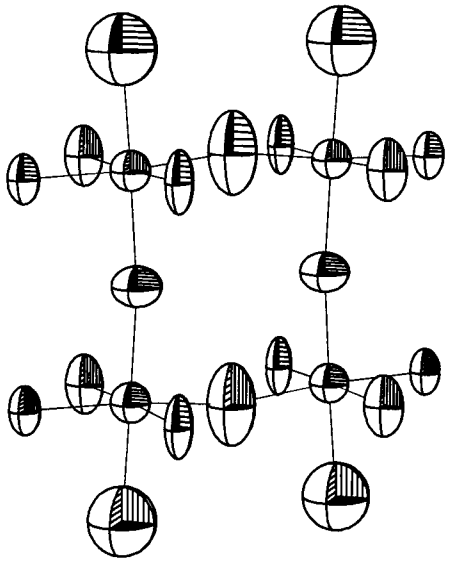

Figure 6. Anisotropic thermal motion (99% ellipsoids) on the oxide sublattice of $Sr_2HoMn_2O_7$ at 290 K; orientation as in Figure 5a.

(19) Battle, P. D.; Gibb, T. C.; Herod, A. J.; Kim, S.-H.; Munns, P. H. *J. Mater. Chem.* **1995**, *5*, 865.

appear to be frozen in the latter, whereas the Ho spins make a paramagnetic contribution to the susceptibility throughout the measured temperature range. This is likely to be due to the different cation distribution over the Sr/Ln sites.

Although the arguments presented above can account for the observed electronic properties of $Sr_2HoMn_2O_7$ and $Sr_2YMn_2O_7$, there is one aspect of our results that we find surprising, namely, the existence of a disordered array of Mn^{3+} and Mn^{4+} cations rather than the formation of a charge-ordered supercell. Charge ordering has been seen at low temperatures in comparable perovskites having the same mean oxidation state for the transition-metal cation, for example, $Pr_{0.5}Sr_{0.5}MnO_3$,[2,20] and also in the K_2NiF_4 structure of $La_{0.5}Sr_{1.5}MnO_4$.[21] Both of these compounds are antiferromagnetic below the charge-ordering temperature. Thus compounds built from single perovskite layers separated by rock-salt layers and compounds built from infinite perovskite blocks show charge ordering, whereas compounds built from double-layer perovskite blocks separated by rock-salt layers apparently do not. The reason for this difference in behavior is not immediately obvious. The presence of charge ordering is often associated with the absence of CMR, but clearly other factors act to suppress the effect in $Sr_2HoMn_2O_7$ and $Sr_2YMn_2O_7$. Although it is known that $Sr_2NdMn_2O_7$ does show CMR, it is not yet clear whether the CMR properties are associated with the spin-glass or antiferromagnetic RP phase in the biphasic material. It has, however, been demonstrated that the spin-glass phase of the perovskite $(Tb_{1/3}La_{2/3})_{2/3}Ca_{1/3}MnO_3$ does show CMR below 120 K.[22] The absence of CMR in RP phases containing the smaller lanthanides[10] is therefore not simply accounted for by the formation of a spin-glass phase and the absence of long-range magnetic order.

All of the above discussion has ignored the presence of ~3% of a perovskite phase in our samples. This will shift the composition of the RP phase away from the ideal stoichiometry and will shift the mean oxidation state of the Mn cations slightly away from the ideal value of 3.5. The X-ray diffraction pattern of the perovskite phase contains only relatively weak peaks, and the impurity phase is therefore easily overlooked unless neutron diffraction data are available. It seems likely that we have never prepared a single-phase RP manganate material and that all our samples have contained either two RP phases, as for Ln = La and Nd, or a single RP phase and a low percentage of perovskite impurity, as for $Sr_2HoMn_2O_7$ and $Sr_2YMn_2O_7$.

In conclusion, we would like to emphasize the main results that come out of this work. We have found two $Sr_2LnMn_2O_7$ compounds which do not show long-range magnetic order above 1.5 K, although there is some evidence of short-range spin ordering. This suggests that competition between antiferromagnetic and ferromagnetic interactions results in frustration. The absence of any significant change in the geometry of the MnO_6 octahedra as a function of temperature is consistent with the fact that the e_g electrons, which are localized at room temperature, remain localized on cooling. There is a marked tilting of the MnO_6 octahedra compared to the ideal RP structure, and this is accompanied by increased nonlinearity of the Mn−O−Mn linkages. Furthermore, the linkage parallel to *z* within the perovskite blocks shows a significant elongation, weakening interactions in this direction and perhaps inducing a certain amount of single-layer (K_2NiF_4-like) character into the compound.

Acknowledgment. We thank the donors of the Petroleum Research Foundation, funded by the American Chemical Society, and the EPSRC for supporting this work. C. C. Tang provided experimental assistance at Daresbury Laboratory.

CM970431P

(20) Knizek, K.; Jirak, Z.; Pollert, E.; Zounova, F.; Vratislav, S. *J. Solid State Chem.* **1992**, *100*, 292.

(21) Sternlieb, B. J.; Hill, J. P.; Wildgruber, U. C.; Luke, G. M.; Nachumi, B.; Moritomo, Y.; Tokura, Y. *Phys. Rev. Lett.* **1996**, *76*, 2169.

(22) DeTeresa, J. M.; Ibarra, M. R.; Garcia, J.; Blasco, J.; Ritter, C.; Algarabel, P. A.; Marquina, C.; delMoral, A. *Phys. Rev. Lett.* **1996**, *76*, 3392.